Electronic Supplementary Material (ESI) for Lab on a Chip.

Electronic Supplementary Information

Endothelial hydraulic conductivity (L_P) measurements

The measured bulk hydraulic permeability (Fig. S1) was used as an input for the computational model of the microfluidic platform to estimate the equivalent hydraulic resistance of the ECM (Fig. S2). The ECM region consists of four flow nodes: the aperture at the BP, the apertures in each BV, and the ECM inlet port. Therefore, the equivalent hydraulic resistances of the ECM include: (i) the resistance between the bifurcation point aperture and the ECM inlet port (R_{BP}) (Fig.S2A), (ii) the resistance between the branched vessel apertures and the ECM inlet port (R_{BV}) (Fig. S2B), (iii) the resistance between the bifurcation point aperture and each branched vessel aperture (R_1) (Fig. S2C), and (iv) the resistance between the branched vessel apertures (R_2) (Fig. S2D). Since the numerically modeled fluid flow rates between each set of flow nodes vary linearly with the level of pressure difference, the interstitial domain can be accurately simplified to a hydraulic network consisting of four nodes using the superposition principle (Fig. S2E). Furthermore, in the presence of HUVECs, the hydraulic resistance of the endothelial monolayer acts serially prior to the resistance of the ECM across the apertures at the BP and in each BV (Fig. S2F).

The transendothelial flux was measured by monitoring the extravasation rate of 10 μM dextran (10 kDa) as a fluorescently tagged solute under 1.5 cm H_2O pressure difference between IVP and IFP (IVP = 1.5 cm H_2O and IFP=0). The net transport of the fluorescent solute was quantified by using the principle of conservation of mass within an Eulerian control volume (Fig. 2A). In other words, the time rate of increase in the total amount of Dextran within the region of interest (i.e., the control volume with differential

element volume of dV) ($\oint C \cdot dV$) normalized by the average intraluminal Dextran concentration (C_{ref}) equates the transendothelial transport rate of Dextran (J_D) (Eq. 1).

$$J_D = \frac{\partial}{\partial t} \oint C \cdot dV \quad (1)$$

To characterize transendothelial transport of a solute such as Dextran, the following membrane transport equation is often employed (Eq .2):

$$J_D/S = P_e \cdot C_{ref} \quad (2)$$

where S in the monolayer area, C_{ref} is the intravascular concentration of Dextran and P_e is the apparent permeability of the endothelial monolayer, which is measured in endothelial permeability assays that involve quantification of transendothelial transport of a fluorescently tagged solute.[1] Apparent permeability of the endothelial monolayer has been previously estimated using the following equation[2] (Eq. 3):

$$P_e = P_0 \cdot Z + (1 - \sigma_s) \cdot J_V \quad (3)$$

where P_0 is the diffusional permeability of Dextran across the endothelium, J_V is total the volumetric flux across the endothelium, σ_s is the drag reflection coefficient, and Z is the non-dimensional parameter indicating the ratio of the convective mode of transendothelial transport over the diffusional mode. The parameter Z is expressed as (Eq. 4):

$$Z = N_{Pe}/(\exp(N_{Pe}) - 1) \quad (4)$$

Where, N_{Pe} is the Peclet number which is defined as (Eq. 5):

$$N_{Pe} = (1 - \sigma_s) \cdot J_V / P_0 \quad (5)$$

The average values of apparent permeability (P_e) measured in our microfluidic system was ~10^{-4} cm/s. The average values of diffusional permeability (P_0) of 10 kDa Dextran, on the order hand, is ~10^{-6} cm/s.[3, 4] Therefore, the value of N_{Pe} throughout our measurements was approximately 100. Due to the large value of Peclet number, the convective mode of the transendothelial transport is dominant over any diffusion effects ($P_e \approx (1 - \sigma_s) \cdot J_V$). The drag reflection coefficient of a solute is dependent on its molecular size. While this coefficient has not been previously reported for Dextran, measurements conducted for α-lactalbumin,[1] which has a molecular weight similar to 10 kDa Dextran, were used in this work (σ_s = 0.35). Therefore, the measured values of apparent permeability for Dextran can be used to estimate the volumetric transendothelial flux (i.e., $P_e \approx 0.65 \times J_V$).

Rewriting Equation 1 in terms of measurable or known parameters, Equation 6 can be used to estimate the total volumetric flux across the endothelial monolayer (Eq. 6):

$$J_V = \frac{1}{0.65 \cdot C_{ref} \cdot S} \times \frac{\partial}{\partial t} \oint C \cdot dV \quad (6)$$

Based on previous reports of a linear correlation between dextran concentration and fluorescence intensity (I) in epifluorescence images ($C_{ref} \propto I_{ref}$ and $C \propto I$),[1, 5] the following equation can be used to quantify the level of volumetric flux across the endothelial monolayer (Eq. 7):

$$J_V = \frac{1}{0.65 \cdot I_{ref} \cdot S} \times \frac{\partial}{\partial t} \oint I \cdot dV \quad (7)$$

Using the estimated ECM hydraulic resistances (Fig. S2), the quantified level of transvascular volumetric flux (J_V) across each aperture (J_{BP}, J_{BV1}, and J_{BV2}) can then be expressed in terms of the extravascular pressure (EVP) that is abluminal to the endothelium at each aperture assuming IFP = 0 (Eqs. 8-10). By writing Equations 8-10 in matrix form (Eq. 11), the values of EVP can be estimated based on the quantified level of volumetric flux across the endothelial monolayer at each aperture. Since the value of IVP is controlled externally (IVP=1.5 cmH_2O), the level of transmural pressure difference can be estimated across the endothelium at each aperture (ΔP=IVP-EVP).

$$J_{BP} \cdot S_{BP} = (R_{BP}^{-1} + 2R_1^{-1}) \cdot EVP_{BP} - R_1^{-1} \cdot EVP_{BV1} - R_1^{-1} \cdot EVP_{BV2} \quad (8)$$

$$J_{BV1} \cdot S_{BV1} = (R_{BV}^{-1} + R_1^{-1} + R_2^{-1}) \cdot EVP_{BV1} - R_1^{-1} \cdot EVP_{BP} - R_2^{-1} \cdot EVP_{BV2} \quad (9)$$

$$J_{BV2} \cdot S_{BV2} = (R_{BV}^{-1} + R_1^{-1} + R_2^{-1}) \cdot EVP_{BV2} - R_1^{-1} \cdot EVP_{BP} - R_2^{-1} \cdot EVP_{BV1} \quad (10)$$

$$\begin{bmatrix} J_{BP} \\ J_{BV1} \\ J_{BV2} \end{bmatrix} = \begin{bmatrix} R_{BP}^{-1} + 2R_1^{-1} & -R_1^{-1} & -R_1^{-1} \\ -R_1^{-1} & R_{BV}^{-1} + R_1^{-1} + R_2^{-1} & -R_2^{-1} \\ -R_1^{-1} & -R_2^{-1} & R_{BV}^{-1} + R_1^{-1} + R_2^{-1} \end{bmatrix} \times \begin{bmatrix} EVP_{BP} \\ EVP_{BV1} \\ EVP_{BV2} \end{bmatrix} \quad (11)$$

The Starling hypothesis was then employed to connect the volumetric flux across the endothelial monolayer[6] to the endothelial hydraulic permeability, L_P and the driving pressure gradient (Eq. 12):

$$J_V = L_P(\Delta P - \sigma \Delta \pi) \quad (12)$$

where ΔP is the hydrostatic pressure difference across the endothelial monolayer, $\Delta\pi$ is the solute oncotic pressure difference across the endothelium, and σ is the reflection coefficient. The oncotic effects are negligible in *in vitro* models of microvasculature due to the homogenous media composition.[7] Therefore, the hydrostatic pressure difference across the endothelial monolayer is the main driving force inducing transvascular flow in this system. Equation 12 is further simplified to the following form:

$$J_V = L_P \cdot \Delta P \quad (13)$$

Thus, the values of ΔP estimated from Eq. 12 along with the estimated volumetric flux levels from Eq. 7 results in the quantification of endothelial hydraulic conductivity (L_P) according to Eq. 13.

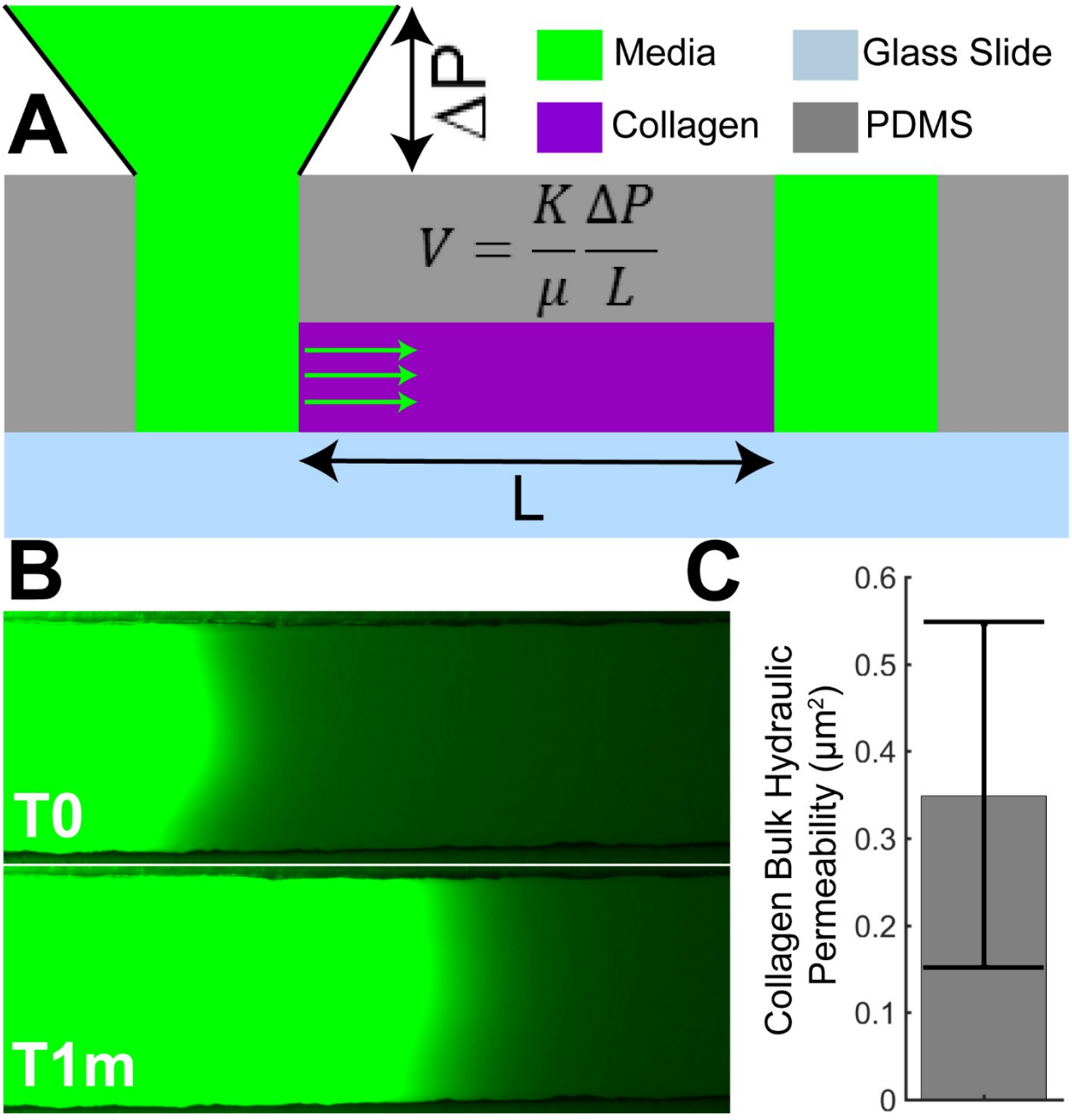

Figure S1. Measurement of bulk hydraulic permeability of the ECM solution using a single channel based microfluidic platform. (A) The schematic of the microfluidic setup. The setup enables the application of controlled level of hydrostatic pressure difference (ΔP) across the microchannel. Assuming Darcy flow, the average velocity of the fluorescently tagged dye (V) divided by ΔP is equal to hydraulic permeability of the

collagen matrix (K) divided by the multiplication of water viscosity (μ) and the microchannel length (L). (B) Representative images of the fluorescently tagged dye inside the microchannel at two different time points. (C) Bulk hydraulic permeability of the ECM solution quantified based on Darcy flow assumption.

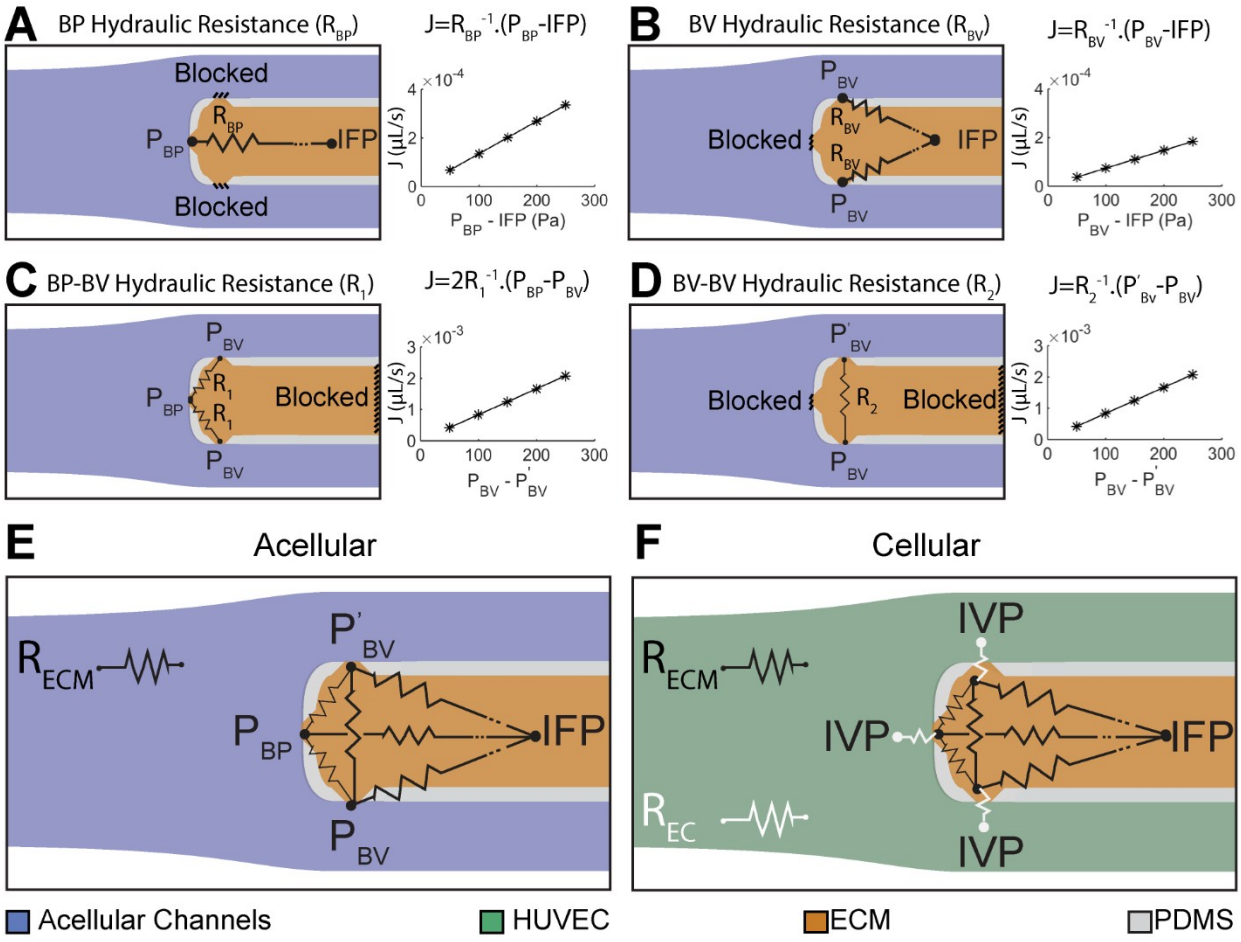

Figure S2. Hydraulic resistance diagram of the acellular and cellular microfluidic model. The hydraulic resistance values (R) were predicted based on the computational model of the microfluidic platform between (A) bifurcation point (BP) aperture and ECM inlet, (B) each branched vessel (BV) aperture and ECM inlet, (C) BP aperture and each BV aperture, and (D) the two BV apertures. The numerically predicted interstitial flow rate (J) between each pair of nodes linearly increased with the level of pressure difference (R^2=1.00 for all four linear fits) confirming the validity of Darcy flow assumption throughout the ECM. (E) The superposed hydraulic resistance diagram of the ECM under acellular

condition. (F) The hydraulic resistance of the HUVEC monolayer paired serially with the ECM hydraulic resistance at each aperture under cellular condition.

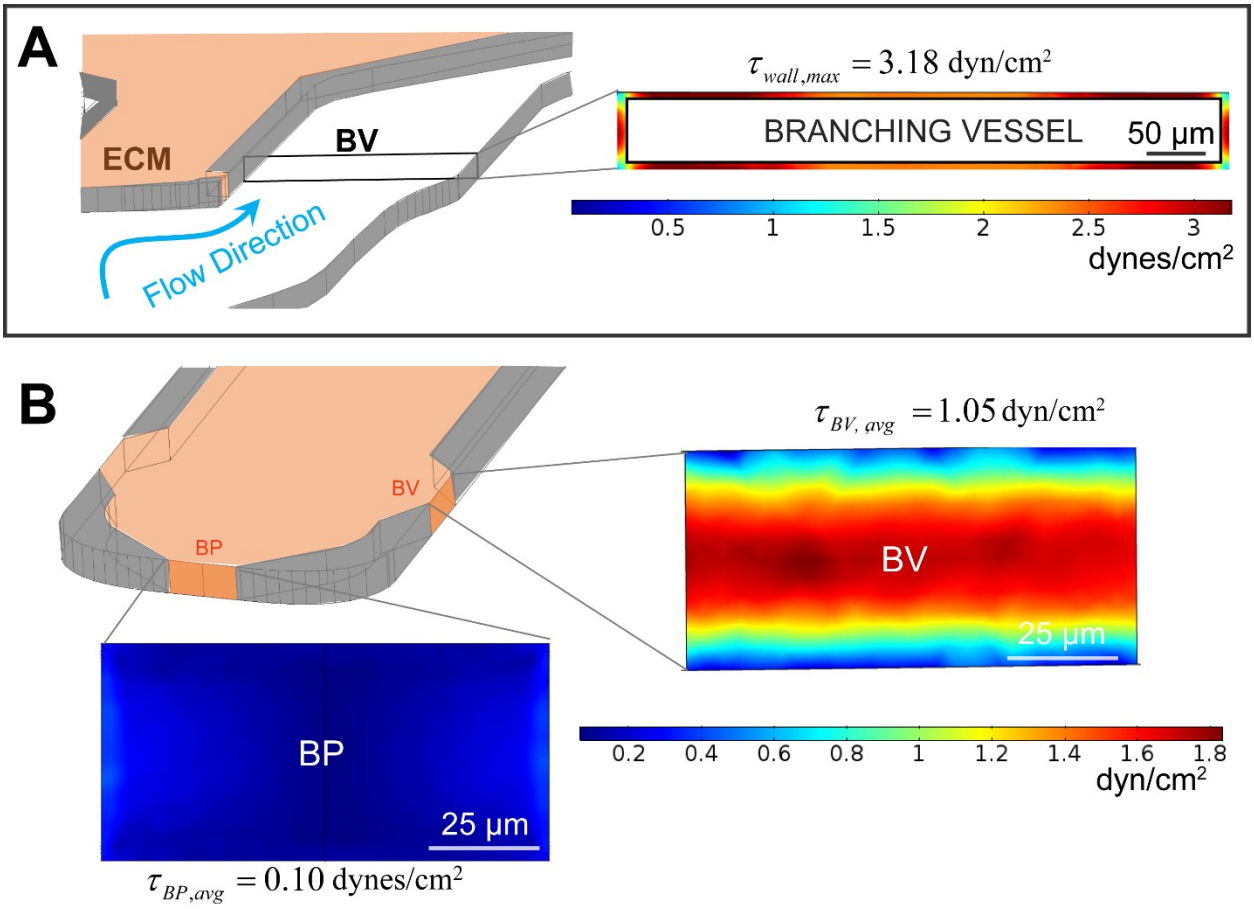

Figure S3. Shear stress distribution at (A) branched vessel and (B) at the bifurcation point and laminar shear stress apertures.

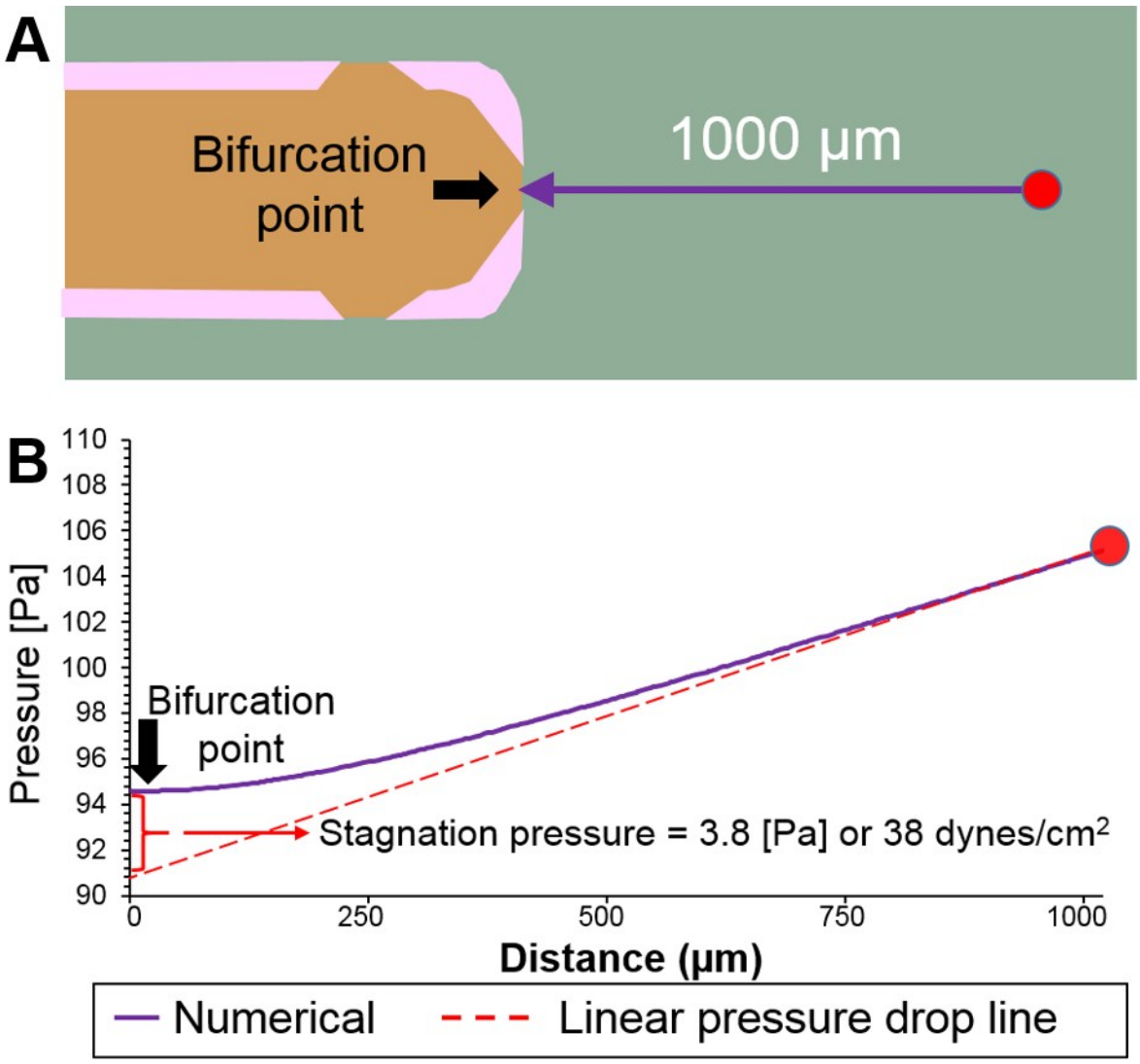

Figure S4. Estimation of stagnation pressure at the bifurcation point (BP). Since the flow is pressure-driven inside the microfluidic device, a linear pressure drop or a constant pressure gradient is experienced as the flow moves from the inlet towards the outlet. As the incoming flow approaches the bifurcation point, the flow decelerates, leading to a gradual pressure build-up, which increases to stagnation pressure at the bifurcation point. (A) Schematic showing the location of bifurcation point where the incoming flow stagnates, and a representative location, 1000 µm from the bifurcation point (red circle)

where local pressure is the free-stream pressure, i.e. no flow stagnation effects are observed. (B) Plot showing the pressure variation from the representative location (red circle) till the bifurcation point, estimated numerically using COMSOL Multiphysics. The difference between the actual pressure and the free-stream pressure at the bifurcation point is the stagnation pressure, with a magnitude of 38 dynes/cm^2 for a flowrate of 10 µL/min.

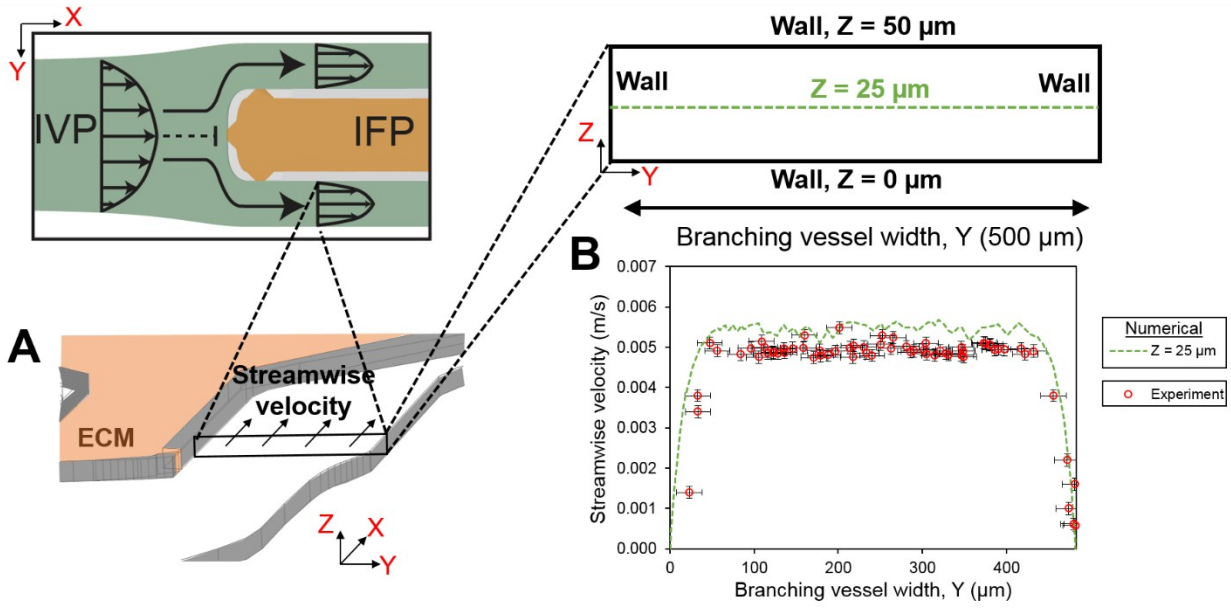

Figure S5. Validation of numerical COMSOL simulations with experiments. (A) Schematic of the microfluidic device depicting the direction of perfusion (along X) in the branched vessel, adjacent to the LSS aperture. For a flow rate of 10 µl/min, peak streamwise velocity for the perfused media was estimate from the numerical simulations in the branched vessel, at Z = 25 µm. Arrows indicate the direction of streamwise velocity along X. (B) Plot showing numerically estimated streamwise velocity distribution of the media, estimated from numerical simulations at Z = 25 µm (dash line). Numerical velocity distribution was validated experimentally by perfusing 4 µm rigid florescent beads at a flow rate of 10 µl/min inside the microfluidic device. The streamwise velocity of the fluorescent particles in the branched vessel was estimated by dividing the streak length of the beads with the exposure time (0.1 s). Estimated experimental velocity profile for rigid particles across various sections of branched vessel correlates with the numerically derived velocity profile at the center of the channel (Z=25µm) . The peak magnitude of the rigid particles is ~10% lower than the peak velocity of the media (fluid) estimated numerically (dash line), and can be attributed to the gradient in shear between the top

and bottom surfaces of the rigid particle[8], producing inertial lift in pressure driven flows, and displacing the equilibrium position of the particle from the center of the channel (Z = 25 μm).

References

1. V. Huxley, F. Curry and R. Adamson, *American Journal of Physiology-Heart and Circulatory Physiology*, 1987, **252**, H188-H197.
2. J. M. Tarbell, *Annu Rev Biomed Eng*, 2003, **5**, 79-118.
3. G. M. Price, K. M. Chrobak and J. Tien, *Microvascular research*, 2008, **76**, 46-51.
4. G. M. Price, K. H. Wong, J. G. Truslow, A. D. Leung, C. Acharya and J. Tien, *Biomaterials*, 2010, **31**, 6182-6189.
5. B. M. Fu, R. H. Adamson and F.-R. E. Curry, *Journal of biomechanical engineering*, 2005, **127**, 270-278.
6. E. H. Starling, *The Journal of physiology*, 1896, **19**, 312-326.
7. M. Turner, *The Journal of physiology*, 1992, **449**, 21-35.
8. D. Di Carlo, *Lab on a Chip*, 2009, **9**, 3038-3046.